AGU PUBLICATIONS

Geophysical Research Letters

RESEARCH LETTER
10.1002/2017GL076849

Key Points:
- Large contribution to El Niño/Southern Oscillation (ENSO)-amplitude diversity in climate models originates from stochastic forcing
- Competing effects in the ENSO dynamics present an important source for ENSO-amplitude diversity
- Due to the importance of stochastic forcing and competing processes, the growth rate of sea surface temperature anomalies must not necessarily correlate with ENSO amplitude

Supporting Information:
- Supporting Information S1
- Data Set S1

Correspondence to:
C. Wengel,
cwengel@geomar.de

Citation:
Wengel, C., Dommenget, D., Latif, M., Bayr, T., & Vijayeta, A. (2018). What controls ENSO-amplitude diversity in climate models? *Geophysical Research Letters*, *45*. https://doi.org/10.1002/2017GL076849

Received 18 DEC 2017
Accepted 10 FEB 2018
Accepted article online 16 FEB 2018

What Controls ENSO-Amplitude Diversity in Climate Models?

C. Wengel[1], D. Dommenget[2], M. Latif[1,3], T. Bayr[1], and A. Vijayeta[2]

[1]GEOMAR Helmholtz Centre for Ocean Research Kiel, Kiel, Germany, [2]School of Earth, Atmosphere and Environment, Monash University, Clayton, Victoria, Australia, [3]Excellence Cluster "The Future Ocean", Kiel University, Kiel, Germany

Abstract Climate models depict large diversity in the strength of the El Niño/Southern Oscillation (ENSO) (ENSO amplitude). Here we investigate ENSO-amplitude diversity in the Coupled Model Intercomparison Project Phase 5 (CMIP5) by means of the linear recharge oscillator model, which reduces ENSO dynamics to a two-dimensional problem in terms of eastern equatorial Pacific sea surface temperature anomalies (T) and equatorial Pacific upper ocean heat content anomalies (h). We find that a large contribution to ENSO-amplitude diversity originates from stochastic forcing. Further, significant interactions exist between the stochastic forcing and the growth rates of T and h with competing effects on ENSO amplitude. The joint consideration of stochastic forcing and growth rates explains more than 80% of the ENSO-amplitude variance within CMIP5. Our results can readily explain the lack of correlation between the Bjerknes Stability index, a measure of the growth rate of T, and ENSO amplitude in a multimodel ensemble.

1. Introduction

The El Niño/Southern Oscillation (ENSO) is the dominant mode of interannual climate variability in the tropics. ENSO is characterized by sea surface temperature (SST) anomalies of a few centigrade primarily in the eastern and central equatorial Pacific, which drive global teleconnections (e.g., Brönnimann et al., 2004). Large diversity among coupled general circulation models (CGCMs) in ENSO statistics such as ENSO amplitude exists (Bellenger et al., 2014; Latif et al., 2001). Understanding the different ENSO dynamics among CGCMs is fundamental for making robust statements about the level of related seasonal climate predictability and uncertainty in long-term ENSO projections.

Over the past years, considerable progress has been made in understanding ENSO diversity in CGCMs by applying conceptual models that condense the dynamics of ENSO into a simple theoretical framework. One example is the Bjerknes Stability (BJ) index (Jin et al., 2006), which approximates the growth rate of SST anomalies (T) in the eastern equatorial Pacific by the recharge oscillator framework (Jin, 1997) and allows examination of the positive and negative feedbacks relevant to ENSO. The BJ index has been used to study ENSO-amplitude diversity among CGCMs (Ferrett & Collins, 2016; Kim et al., 2014; Kim & Jin, 2011). A recent study by An et al. (2017) showed that the diversity in the thermocline feedback is highly correlated to ENSO-amplitude diversity. The BJ index has also been used to study potential ENSO changes in a warmer climate (Ferrett & Collins, 2016; Kim & Jin, 2011). In theory, a larger BJ index is associated with larger ENSO amplitude. Kim et al. (2014) have shown that the BJ index is correlated to ENSO amplitude in models from the Coupled Model Intercomparison Project Phase 3 (CMIP3). However, this correlation breaks down in models participating in CMIP5 (due to a few outliers). One possible explanation is that nonlinear dynamics are not represented by the BJ index (Graham et al., 2014). Further, the potential influence from atmospheric noise has been discussed in this context (Ferrett & Collins, 2016).

Another powerful tool for investigating ENSO diversity among models is the simplest version of the recharge oscillator model of Burgers et al. (2005) (ReOsc model hereafter). The growth mechanism in this model is due to a positive coupled feedback (Bjerknes, 1969), whereas the oscillatory component is driven by the recharge-discharge of equatorial ocean heat content (Cane & Zebiak, 1985; Wyrtki, 1975, 1986). This dynamical framework can be described by a damped harmonic oscillator (Burgers et al., 2005) with SST and thermocline depth playing the roles of momentum and position, respectively. The oscillatory nature of ENSO allows the ReOsc model to capture important characteristics of ENSO dynamics. Many studies have used the ReOsc model to analyze ENSO dynamics in various approaches (Burgers et al., 2005; Frauen & Dommenget, 2010; Jansen et al., 2009; Jin et al., 2007; Levine & McPhaden, 2015; Vijayeta & Dommenget, 2017; Yu et al., 2016). In contrast to the one-dimensional framework underlying the BJ index, the ReOsc model is based on two coupled

equations in which six parameters, including stochastic noise forcing (hereafter stochastic forcing), control ENSO amplitude.

In this paper, the ReOsc model is used to investigate ENSO-amplitude diversity in CMIP5 models. We investigate the relative importance of the ReOsc model parameters for ENSO amplitude with a special focus on the role of stochastic forcing for ENSO-amplitude diversity among CMIP5 models.

2. Data and Methods

We analyze the historical experiments from 35 CMIP5 models (Taylor et al., 2012) for the time period from 1921 to 2000 (Table S1). Output from the Simple Ocean Data Assimilation (SODA) ocean reanalysis product version 2.0.2 (Carton & Giese, 2008) for the period 1958–2001 is used for comparison.

The ReOsc model describes the oscillatory behavior of ENSO by the interaction of eastern equatorial Pacific SST and equatorial Pacific zonal-mean upper ocean heat content:

$$\frac{dT}{dt} = a_{11} \cdot T + a_{12} \cdot h + \xi_T \tag{1}$$

$$\frac{dh}{dt} = a_{21} \cdot T + a_{22} \cdot h + \xi_h \tag{2}$$

where T is the monthly eastern equatorial Pacific SST anomaly; h is the monthly equatorial Pacific zonal-mean thermocline depth anomaly, which is commonly used to approximate the upper ocean heat content anomaly; a_{11} and a_{22} are the growth rate of T and h, respectively; a_{12} and a_{21} are the coupling of T to h and h to T, respectively; and ξ_T and ξ_h are stochastic forcing terms of T and h, respectively. T is averaged here over the Niño3.4-region (170°W–120°W; 5°S–5°N), and h is averaged across the equatorial Pacific (130°E–80°W; 5°S–5°N). The ReOsc model parameters a_{11}, a_{12}, a_{21}, and a_{22} are estimated via multivariate linear regression of the T and h tendencies against T and h, respectively. The stochastic forcing terms are approximated as the standard deviation (SD) of the residuals of the fit, which also may contain dynamics that cannot purely be considered as noise in the sense that they are independent of the large-scale coupled dynamics. We note that the stochastic forcing could be further separated into a state-dependent and a state-independent part (Levine et al., 2016). This, however, would be beyond the scope of this paper. Following Kim et al. (2014) we approximate ENSO amplitude by the SD of T.

The parameter a_{11} is influenced by a number of atmospheric and oceanic processes (Frauen & Dommenget, 2010; Vijayeta & Dommenget, 2017; Yu et al., 2016) such as the Bjerknes feedback and atmospheric heat fluxes as well as ocean dynamics such as mixing and advection. In general, a_{22} is assumed to be close to zero as changes in h are not determined by the thermocline depth itself but rather by the geostrophic response to wind stress (Burgers et al., 2005). On the other hand, a damping of h can be achieved via wave-friction as in the delayed action oscillator model (Suarez & Schopf, 1988). The oscillatory behavior of the ReOsc model is determined by the coupling between T and h, whereby a_{12} is the local warming effect of h on T and a_{21} is the influence of T on h via the atmospheric bridge. Parameter ξ_T is the stochastic forcing of T primarily related to westerly wind bursts, whereas ξ_h is supposed to be largely influenced by ξ_T as both terms are correlated (see below). The stochastic forcing introduces an irregularity to the harmonic oscillation.

The ReOsc model equations can be integrated with stochastic forcing terms to generate time series of T and h using fixed values for a_{11}, a_{12}, a_{21}, and a_{22}. We use a time step of 24 hr and assumed red-noise stochastic forcing terms ξ_T and ξ_h with a decorrelation time of 3 days, mimicking weather systems, which effectively results in white noise forcing when considering monthly means. Identical stochastic forcing is used in all integrations, which allows us to discuss changes of T as functions of parameter changes without any uncertainties resulting from the noise. The integration length of all experiments is 1000 years. Prior to analysis, the linear trend was subtracted from all data and anomalies of T and h were obtained by subtracting the climatological seasonal cycle.

3. Results

The relative importance of the growth rates, coupling, and stochastic forcing terms, as represented by the six ReOsc model parameters, in determining ENSO amplitude is investigated in the CMIP5 model ensemble

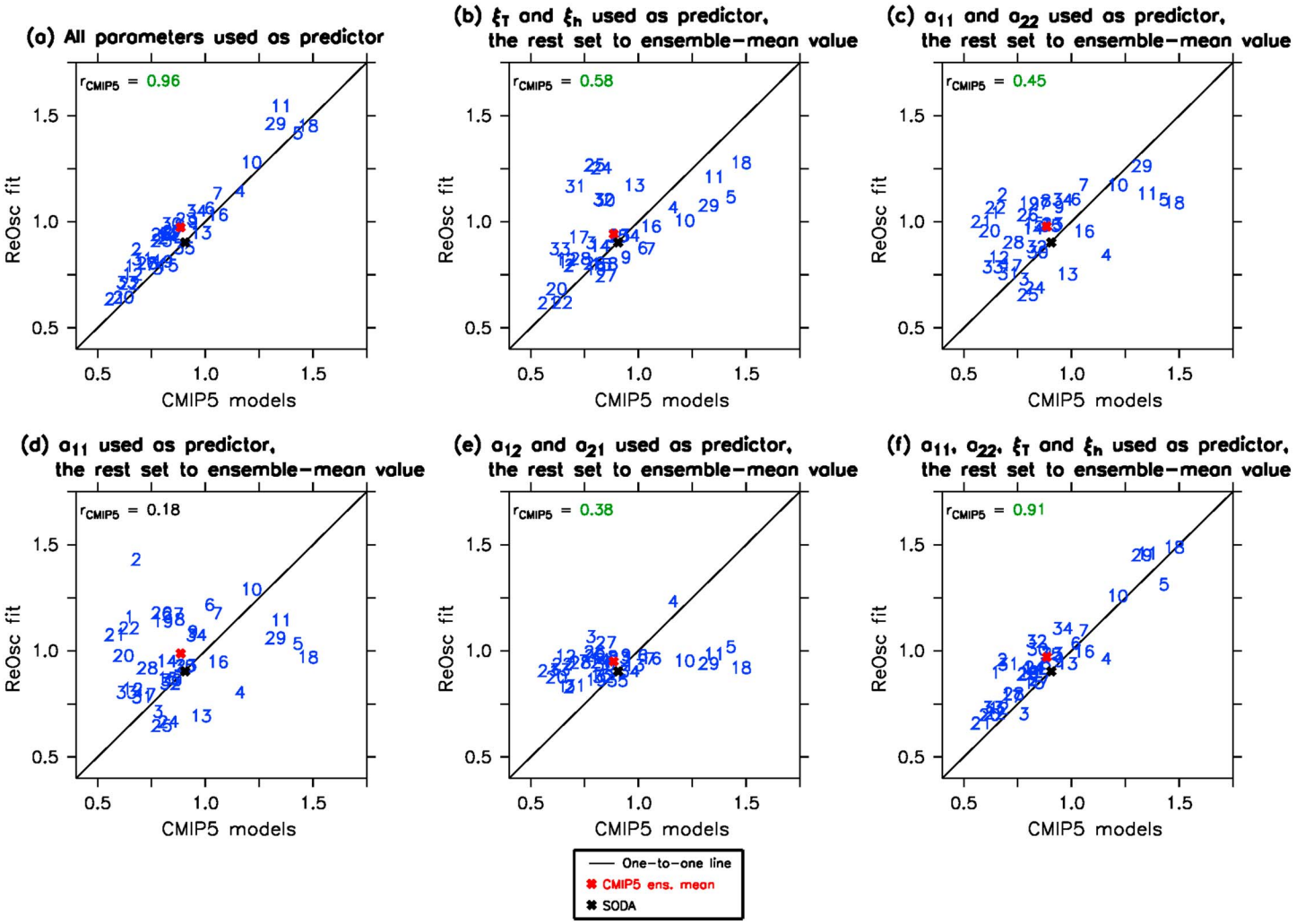

Figure 1. Scatter plots of El Niño/Southern Oscillation (ENSO) amplitude (K) as simulated by the Coupled Model Intercomparison Project Phase 5 (CMIP5) models (horizontal axes) and that obtained from integrating the recharge oscillator (ReOsc) model with parameters estimated for each CMIP5 model (vertical axis) where (a) all six ReOsc parameters are used for the integration, (b) only ξ_T and ξ_h are used, (c) only a_{11} and a_{22}, (d) only a_{11}, (e) only a_{12} and a_{21}, and (f) only a_{11}, a_{22}, ξ_T, and ξ_h with the other parameters set fixed at the ensemble-mean values. Shown are also the CMIP5 ensemble-mean (red cross) and Simple Ocean Data Assimilation (SODA) (black cross), the linear correlation coefficient over all CMIP5 models in the upper left corner of each figure panel (values marked in green indicate statistical significance at the 95%) and the diagonal (black line).

(Figure 1). We compare ENSO amplitude obtained from integrating the ReOsc model using the parameters estimated separately for each CMIP5 model with that directly calculated from each model (Figure 1a). All models are located near the diagonal with a correlation coefficient of 0.96, implying that the ReOsc model is capable to reproduce ENSO amplitude with the respective parameters from each model. We then repeated the integrations by only using from each model the stochastic forcing terms ξ_T and ξ_h (Figure 1b), the respective growth rates a_{11} and a_{22} (Figure 1c) and a_{11} (Figure 1d), and the coupling terms a_{12} and a_{21} (Figure 1e) while keeping the other parameters fixed at the ensemble-mean value. The results suggest that the largest influence on ENSO amplitude originates from the stochastic forcing terms of T and h with a correlation of 0.58. The stochastic forcing term exhibits a large variability among the CMIP5 models, while it is quite constant in time within each individual CMIP5 simulation. The model spread is roughly three times larger than the temporal variability within each individual CMIP5 model simulation (Table S2). Second largest influence on ENSO amplitude is due to the growth rates of T and h with a correlation of 0.45. When only varying the growth rate of T (a_{11}), the variation of ENSO amplitude is large but the correlation is very low (0.18). The integrations of the ReOsc model by only using the coupling parameters from each CMIP5 model yields very little variation in ENSO amplitude. The combined variation of the growth rates and the stochastic

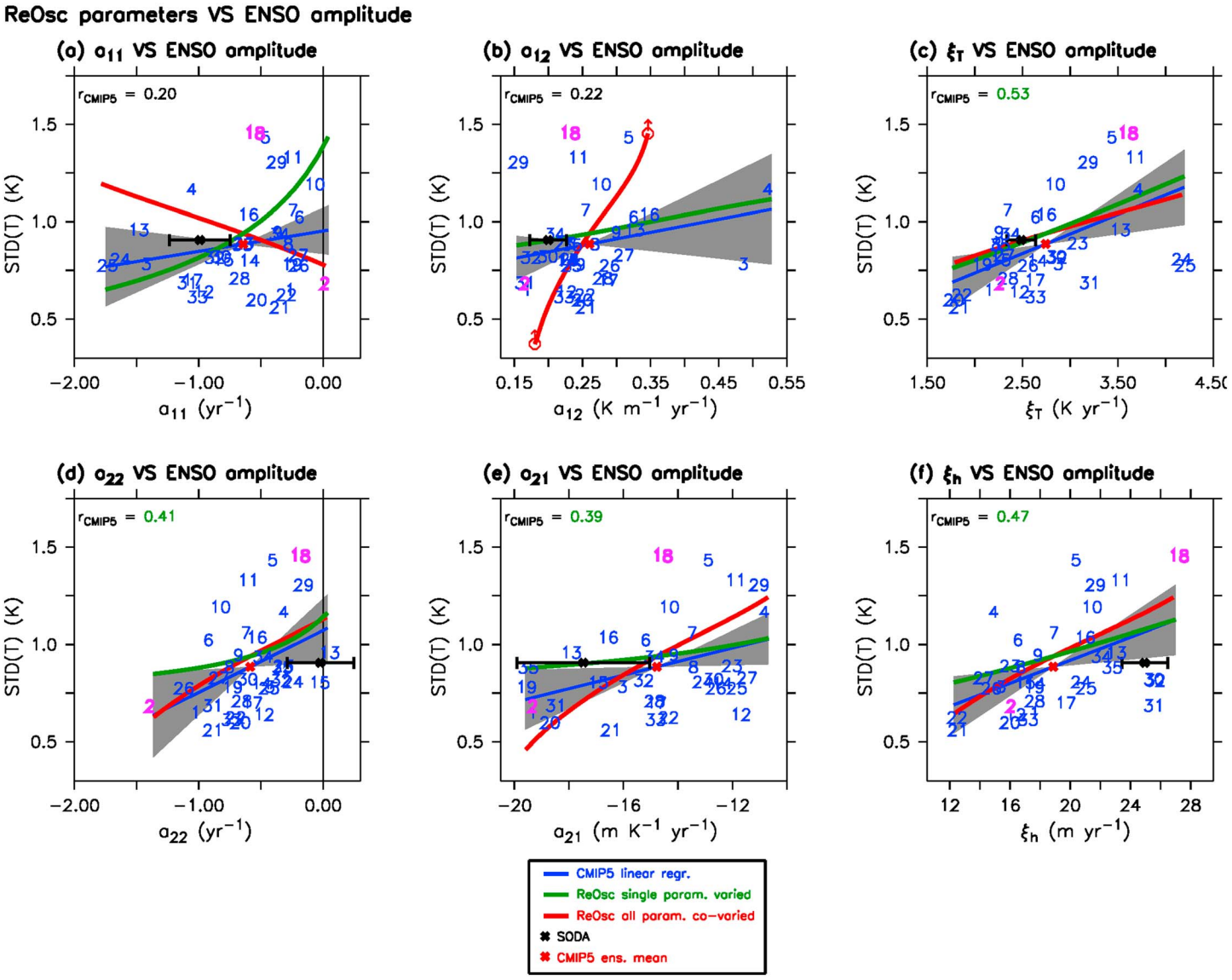

Figure 2. Scatter plot of El Niño/Southern Oscillation (ENSO) amplitude versus the (a) growth rate of T (a_{11}), (b) coupling of T to h (a_{12}), (c) stochastic forcing of T (ξ_T), (d) growth rate of h (a_{22}), (e) coupling of h to T (a_{21}), and (f) stochastic forcing of h (ξ_h) in the Coupled Model Intercomparison Project Phase 5 (CMIP5) models (blue numbers), the CMIP5 ensemble mean (red cross), and Simple Ocean Data Assimilation (SODA) (black cross with 95% confidence interval). The linear correlation coefficient over all CMIP5 models is given in the upper left corner of each figure panel (statistically significant values at the 95% level are shown in green), and a linear regression line is added (blue line) with a 95% uncertainty range (gray shading). Also shown is ENSO amplitude obtained from integrating the recharge oscillator (ReOsc) model as a function of a single parameter (green graph) and as a function of covarying parameters based on EOF-1 (red graph). The red circles with an upward arrow in (b) illustrate infinite growth of ENSO amplitude (see text for details). CMIP5 models 2 and 18 are highlighted in magenta for discussion (see text).

forcing terms (Figure 1f) yields a correlation of 0.91, which is very similar to the case in which all six parameters were varied. Thus, besides the stochastic forcing, the growth rates of T and h are important factors in controlling ENSO-amplitude diversity in CMIP5.

We next compare ENSO amplitude in the CMIP5 model ensemble and as derived from SODA (black cross) with the parameters a_{11}, a_{12}, a_{21}, a_{22}, ξ_T, and ξ_h estimated separately for each model (Figure 2, blue numbers). The uncertainty of the estimated parameters from each individual CMIP5 model (Table S3) is on average smaller than the uncertainty estimated from SODA (black horizontal error bar), which in turn is much smaller than the model spread in CMIP5. In CMIP5, the growth rate of T (a_{11}) shows no significant correlation with ENSO amplitude (Figure 2a), which is consistent with the results from Kim et al. (2014) applying the BJ index. Both a_{11} and the BJ index are estimates of the growth rate of T.

Table 1
ReOsc Parameter Cross Correlations in CMIP5

	Cross correlations					
	a_{11}	a_{12}	a_{21}	a_{22}	ξ_T	ξ_h
a_{11}		−0.18	−0.07	**−0.57**	**−0.58**	−0.26
a_{12}			0.20	0.17	0.17	**−0.34**
a_{21}				0.23	**0.44**	−0.07
a_{22}					**0.49**	**0.38**
ξ_T						**0.52**

Note. Correlation values marked in bold indicate statistical significance at the 95% level.

The relationship between each single ReOsc parameter and ENSO amplitude is modeled by a set of ReOsc model integrations. Each parameter is varied separately to cover the full range in CMIP5, while the other parameters are set to the ensemble-mean values (see section 2 for details). The results (green lines in Figures 2a–2f) are quite different from the linear relationships obtained from the CMIP5 models themselves (blue line in Figures 2a–2f), especially for the growth rates a_{11} (Figure 2a) and to a lesser extent a_{22} (Figure 2d).

The combined effect of all parameters ultimately determines the ENSO amplitude in each CMIP5 model. There are significant cross relationships between the variations of the ReOsc parameters within the CMIP5 ensemble, as shown by their cross correlations (Table 1). Largest anticorrelation is found between a_{11} and a_{22} (−0.57) as well as between a_{11} and ξ_T (−0.58) and largest positive correlation between ξ_T and ξ_h (0.52). This suggests the presence of competing ENSO processes, which previously has been discussed in terms of ENSO feedbacks (e.g., Bayr et al., 2017; Bellenger et al., 2014; Lloyd et al., 2009). These studies addressed the compensation between the too weak positive zonal wind feedback and the too weak negative heat flux feedback observed in most climate models, which possibly is reflected by the anticorrelation of a_{11} with a_{22} and ξ_T. The heat flux feedback is contributing to a_{11} (Frauen & Dommenget, 2010), and changes in h and hence in a_{22} are mainly governed by the geostrophic response to wind stress (Burgers et al., 2005). Further, ξ_T is driven by atmospheric noise primarily associated with westerly wind bursts. However, a detailed analysis of the origin of these covariations is beyond the scope of this paper.

To investigate the impact of the competing processes on ENSO amplitude, we extract modes of covariance from the ReOsc model parameters (Figure 3) by performing an empirical orthogonal function (EOF) analysis, with the six ReOsc model parameters as one dimension and the individual CMIP5 models as the other dimension. The leading mode (EOF-1) explains 42% of the parameter variability (Figure 3a). Consistent with the most significant cross correlations (Table 1), EOF-1 describes covariability between a_{11} and a_{22}, between a_{11} and ξ_T with opposite signs (Figure 3b), and between ξ_T and ξ_h with the same sign. Explained variances for each parameter are depicted in Figure 3c. EOF-1 explains largest variance in a_{11} (59%), a_{22} (63%), and ξ_T (77%), whereas it explains less variance in ξ_h (31%) and low variance in a_{12} (4%) and a_{21} (17%). EOF-2, on the other hand, accounts for the largest explained variance in a_{12} (67%), a_{21} (26%), and ξ_h (50%) but only less than 1% in the other parameters.

The sensitivity of ENSO amplitude to the covariability given by EOF-1 can be estimated by scaling the EOF-1 pattern (Figure 3b) over the range of a_{11}. Using this new set of parameters, the ReOsc model is again

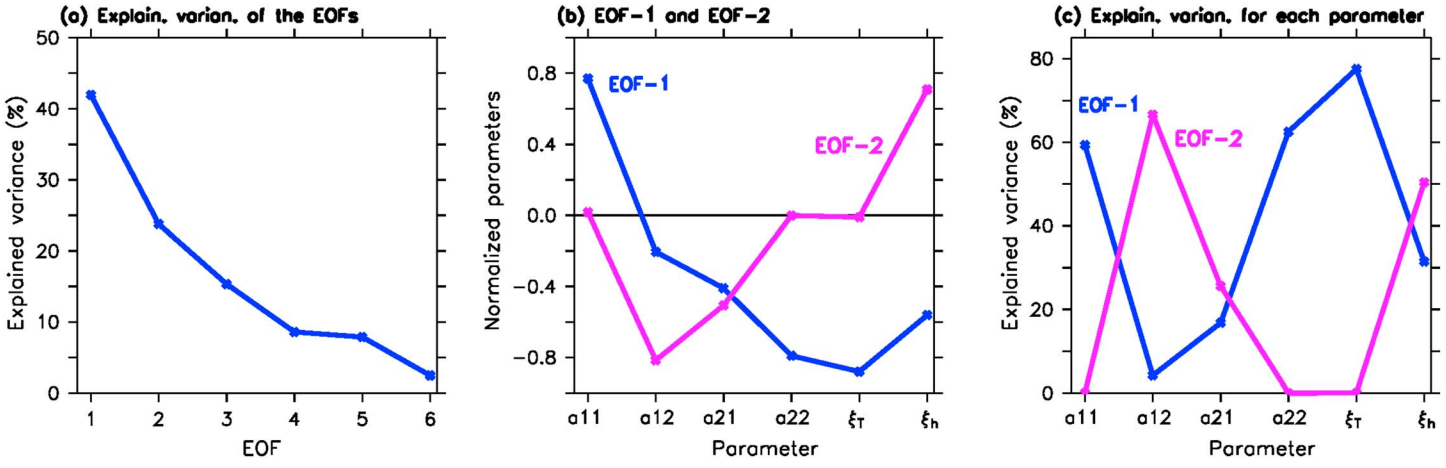

Figure 3. Results from the empirical orthogonal function (EOF) analysis of recharge oscillator parameters in the Coupled Model Intercomparison Project Phase 5. Shown are (a) the explained variances of the EOFs, (b) EOF-1 and EOF-2 (normalized by the standard deviation of the parameters), and (c) the explained variances of EOF-1 and EOF-2 for each parameter.

integrated and ENSO-amplitude dependence calculated (red line in Figures 2a–2f). The covariation among the parameters as given by EOF-1 leads to a dramatic change of ENSO-amplitude dependence on the ReOsc model parameters (red lines in Figures 2a–2f). For example, ENSO amplitude decreases with larger values of a_{11} (red line in Figure 2a), which is the opposite relationship as if only a_{11} is varied (green line). Considering the covariability among the parameters reduces the root-mean-square errors (Table S4). This demonstrates a significant influence of competing processes on ENSO amplitude, mainly between a_{11}, a_{22}, and ξ_T.

We illustrate the impact of the competing processes for specific models using the growth rate of T (a_{11}) as a first guess of ENSO amplitude. For example, the Australian Community Climate and Earth System Simulator 1.3 (ACCESS1.3) model exhibits rather small ENSO amplitude compared to the other models and SODA (black cross), although a_{11} is largest (magenta number 2 in Figure 2a).On the other hand, the growth rate of the thermocline depth perturbation h (a_{22}) is small in ACCESS1.3 (Figure 2d) as are the coupling terms (Figures 2b and 2e). Further, there are rather small stochastic forcing terms in ACCESS1.3 (Figures 2c and 2f). Altogether, this may explain why ENSO amplitude is unexpectedly small in this model. Another interesting example is the Geophysical Fluid Dynamics Laboratory Earth System Model 2M, which exhibits the largest ENSO amplitude but not exceptionally large a_{11} (magenta number 18 in Figure 2a). In this model, the growth rate of h (a_{22}) is high as are the two stochastic forcing terms. It is this combination that leads to large ENSO amplitude. Our results suggest that competing ENSO processes is a key to explain ENSO-amplitude diversity in the CMIP5 model ensemble and that the growth rate of T (a_{11}) alone cannot explain the diversity.

With respect to the coupling parameter a_{12}, the ReOsc model with the covariability of EOF-1 included becomes unstable for certain parameter values and ENSO amplitude grows to infinity, which is illustrated in Figure 2b (red circle with upward arrow). This is because EOF-1 explains only a small fraction of the total variance in a_{12}. Variations in this parameter are better modeled by EOF-2 (not shown), as suggested by Figure 3c.

We also repeated the analysis for those CMIP5 models that were selected by Kim et al. (2014), for a set of perturbed physics simulations with the Kiel Climate Model (Park et al., 2009; Wengel et al., 2017) and for the CMIP3 models (Figures S1–S9 and Tables S5–S13). Qualitatively, the results from the KCM and CMIP3 ensembles are very similar to the CMIP5 results presented here. The stochastic forcing, however, explains less variance in ENSO-amplitude diversity in the former two ensembles relative to CMIP5, but the combined variation of the stochastic forcing and the growth rate again explains the largest fraction of the spread as in CMIP5. Further, the growth rate of T (a_{11}) explains less variance in the parameter space in CMIP3 in comparison to CMIP5 and yields slightly different behavior with respect to the competing processes.

4. Conclusions

We have investigated ENSO-amplitude diversity in models from the CMIP5 within the framework of the linear ReOsc model. The model involves six parameters representing the growth rates of the eastern equatorial Pacific sea surface temperature anomaly (T) and equatorial Pacific upper ocean heat content anomaly (h), the mutual coupling and stochastic forcing of T and h. The ReOsc model has the form of a damped harmonic oscillator with T and h playing the roles of momentum and position, respectively. Regardless of the ReOsc models' simplicity, it can well represent ENSO statistics in reanalysis data (SODA) and climate models.

A large fraction contributing to ENSO-amplitude diversity in the CMIP5 model ensemble is due to variations in stochastic forcing (34%). This was shown by comparing ENSO amplitudes calculated from the CMIP5 models themselves with those obtained from ReOsc model integrations when only taking into account the effect of stochastic forcing. This finding relates to the limited predictability of El Niño and La Niña events due to the chaotic nature of high-frequency variability (Eckert & Latif, 1997). Relatively large influence on ENSO-amplitude diversity also originates from the growth rates of T and h (20%), whereas their coupling strength is of minor influence. The combined effect of stochastic forcing and the growth rates explains more than 80% of the variance in ENSO amplitude.

Further analysis revealed competing effects in the ENSO dynamics of the CMIP5 models, primarily between the growth rates of T and h, and the stochastic forcing of T. The competing processes present an important source for ENSO-amplitude modulations in climate models. This was shown by integrating the ReOsc model

for a range of parameters, with and without taking into account the effects of the competing processes, and comparing the results with those directly obtained from the CMIP5 models. The effect of changes in the growth rate of *T* on ENSO amplitude is largely offset by that of the growth rate of *h* and by the stochastic forcing of *T*. The cause of these dynamic cross relations is unclear at this point but presents an interesting aspect of ENSO dynamics and requires further investigation. The possible relation to ENSO feedback compensation has been noted (Bayr et al., 2017; Bellenger et al., 2014; Lloyd et al., 2009).

We find that the growth rate of *T* from the ReOsc model only explains a very little fraction of ENSO-amplitude variance. Further, the growth rate does not significantly correlate with ENSO amplitude in CMIP5. This is consistent with the finding by Kim et al. (2014), who applied the BJ index, which approximates the growth rate of *T* in terms of positive and negative ENSO feedbacks. We show that the effects of stochastic forcing and competing processes are important factors contributing to ENSO-amplitude diversity. Since the BJ index does not account for these effects, it must not necessarily correlate with ENSO amplitude.

Acknowledgments
This work was supported by the Integrated School of Ocean Sciences (ISOS) at the Excellence Cluster "The Future Ocean" at Kiel University, the German Ministry of Education and Research (BMBF) grant SACUS (03G0837A) and EU FP7/2007–2013 under grant agreement 603521, project PREFACE, the ARC Centre of Excellence for Climate System Science, Australian Research Council (grant CE110001028), and SFB 754 "Climate-Biochemistry Interactions in the tropical Ocean." We thank two anonymous reviewers for helpful comments and feedback on this work. We acknowledge the World Climate Research Programme's Working Group on Coupled Modeling, which is responsible for CMIP, and we thank the climate modeling groups (listed in Table S1 in the supporting information of this paper) for producing and making available their model output. The CMIP5 data output is available at http://www.ipcc-data.org/sim/gcm_monthly/AR5/Reference-Archive.html. For CMIP the U.S. Department of Energy's Program for Climate Model Diagnosis and Intercomparison provides coordinating support and led development of software infrastructure in partnership with the Global Organization for Earth System Science Portals. The processed CMIP5 data used for this paper are available in the supporting information. Data presented in the supporting information can be provided upon request. The supplementary climate model integrations with the Kiel Climate Model were performed at the Computing Centre of Kiel University. This study is a contribution to the Cluster of Excellence "The Future Ocean."

References

An, S.-I., Heo, E. S., & Kim, S. T. (2017). Feedback process responsible for intermodel diversity of ENSO variability. *Geophysical Research Letters*, *44*, 4272–4279. https://doi.org/10.1002/2017GL073203

Bayr, T., Latif, M., Dommenget, D., Wengel, C., Harlaß, J., & Park, W. (2017). Mean-state dependence of ENSO atmospheric feedbacks in climate models. *Climate Dynamics*. https://doi.org/10.1007/s00382-017-3799-2

Bellenger, H., Guilyardi, E., Leloup, J., Lengaigne, M., & Vialard, J. (2014). ENSO representation in climate models: From CMIP3 to CMIP5. *Climate Dynamics*, *42*(7-8), 1999–2018. https://doi.org/10.1007/s00382-013-1783-z

Bjerknes, J. (1969). Atmospheric teleconnections from the equatorial Pacific. *Monthly Weather Review*, *97*(3), 163–172. https://doi.org/10.1175/1520-0493(1969)097%3C0163:ATFTEP%3E2.3.CO;2

Brönnimann, S., Luterbacher, J., Staehelin, J., Svendby, T. M., Hansen, G., & Svenøe, T. (2004). Extreme climate of the global troposphere and stratosphere in 1940–42 related to El Niño. *Nature*, *431*(7011), 971–974. https://doi.org/10.1038/nature02982

Burgers, G., Jin, F. F., & van Oldenborgh, G. J. (2005). The simplest ENSO recharge oscillator. *Geophysical Research Letters*, *32*, L13706. https://doi.org/10.1029/2005GL022951

Cane, M. A., & Zebiak, S. E. (1985). A theory for El Niño and the southern oscillation. *Science*, *228*, 1084–1087.

Carton, J. A., & Giese, B. S. (2008). A reanalysis of ocean climate using simple ocean data assimilation (SODA). *Monthly Weather Review*, *136*(8), 2999–3017. https://doi.org/10.1175/2007MWR1978.1

Eckert, C., & Latif, M. (1997). Predictability of a stochastically forced hybrid coupled model of El Niño. *Journal of Climate*, *10*(7), 1488–1504. https://doi.org/10.1175/1520-0442(1997)010%3C1488:POASFH%3E2.0.CO;2

Ferrett, S., & Collins, M. (2016). ENSO feedbacks and their relationships with the mean state in a flux adjusted ensemble. *Climate Dynamics*, 1–20. https://doi.org/10.1007/s00382-016-3270-9

Frauen, C., & Dommenget, D. (2010). El Niño and la Niña amplitude asymmetry caused by atmospheric feedbacks. *Geophysical Research Letters*, *37*, L18801. https://doi.org/10.1029/2010GL044444

Graham, F. S., Brown, J. N., Langlais, C., Marsland, S. J., Wittenberg, A. T., & Holbrook, N. J. (2014). Effectiveness of the Bjerknes stability index in representing ocean dynamics. *Climate Dynamics*, *43*(9-10), 2399–2414. https://doi.org/10.1007/s00382-014-2062-3

Jansen, M. F., Dommenget, D., & Keenlyside, N. (2009). Tropical atmosphere-ocean interactions in a conceptual framework. *Journal of Climate*, *22*(3), 550–567. https://doi.org/10.1175/2008JCLI2243.1

Jin, F.-F. (1997). An equatorial ocean recharge paradigm for ENSO. Part I: Conceptual model. *Journal of the Atmospheric Sciences*, *54*(7), 811–829. https://doi.org/10.1175/1520-0469(1997)054%3C0811:AEORPF%3E2.0.CO;2

Jin, F.-F., Kim, S. T., & Bejarano, L. (2006). A coupled-stability index for ENSO. *Geophysical Research Letters*, *33*, L23708. https://doi.org/10.1029/2006GL027221

Jin, F.-F., Lin, L., Timmermann, A., & Zhao, J. (2007). Ensemble-mean dynamics of the ENSO recharge oscillator under state-dependent stochastic forcing. *Geophysical Research Letters*, *34*, L03807. https://doi.org/10.1029/2006GL027372

Kim, S. T., Cai, W., Jin, F.-F., & Yu, J.-Y. (2014). ENSO stability in coupled climate models and its association with mean state. *Climate Dynamics*, *42*(11-12), 3313–3321. https://doi.org/10.1007/s00382-013-1833-6

Kim, S. T., & Jin, F. F. (2011). An ENSO stability analysis. Part II: Results from the twentieth and twenty-first century simulations of the CMIP3 models. *Climate Dynamics*, *36*(7-8), 1609–1627. https://doi.org/10.1007/s00382-010-0872-5

Latif, M., Sperber, K., Arblaster, J., Braconnot, P., Chen, D., Colman, A., et al. (2001). ENSIP: The El Niño simulation intercomparison project. *Climate Dynamics*, *18*(3-4), 255–276. https://doi.org/10.1007/s003820100174

Levine, A., Jin, F.-F., & McPhaden, M. J. (2016). Extreme noise–extreme El Niño: How state-dependent noise forcing creates El Niño–La Niña asymmetry. *Journal of Climate*, *29*(15), 5483–5499. https://doi.org/10.1175/JCLI-D-16-0091.1

Levine, A. F. Z., & McPhaden, M. J. (2015). The annual cycle in ENSO growth rate as a cause of the spring predictability barrier. *Geophysical Research Letters*, *42*, 5034–5041. https://doi.org/10.1002/2015GL064309

Lloyd, J., Guilyardi, E., Weller, H., & Slingo, J. (2009). The role of atmosphere feedbacks during ENSO in the CMIP3 models. *Atmospheric Science Letters*, *10*(3), 170–176. https://doi.org/10.1002/asl.227

Park, W., Keenlyside, N., Latif, M., Ströh, A., Redler, R., Roeckner, E., & Madec, G. (2009). Tropical Pacific climate and its response to global warming in the Kiel climate model. *Journal of Climate*, *22*(1), 71–92. https://doi.org/10.1175/2008JCLI2261.1

Suarez, M. J., & Schopf, P. S. (1988). A delayed action oscillator for ENSO. *Journal of the Atmospheric Sciences*, *45*(21), 3283–3287. https://doi.org/10.1175/1520-0469(1988)045%3C3283:ADAOFE%3E2.0.CO;2

Taylor, K. E., Stouffer, R. J., & Meehl, G. A. (2012). An overview of CMIP5 and the experiment design. *Bulletin of the American Meteorological Society*, *93*(4), 485–498. https://doi.org/10.1175/BAMS-D-11-00094.1

Vijayeta, A., & Dommenget, D. (2017). An evaluation of ENSO dynamics in CMIP simulations in the framework of the recharge oscillator model. *Climate Dynamics*. https://doi.org/10.1007/s00382-017-3981-6

Wengel, C., Latif, M., Park, W., Harlaß, J., & Bayr, T. (2017). Seasonal ENSO phase locking in the Kiel climate model: The importance of the equatorial cold sea surface temperature bias. *Climate Dynamics*. https://doi.org/10.1007/s00382-017-3648-3

Wyrtki, K. (1975). El Niño - the dynamic response of the equatorial Pacific Ocean to atmospheric forcing. *Journal of Physical Oceanography*, *5*(4), 572–584. https://doi.org/10.1175/1520-0485(1975)005%3C0572:ENTDRO%3E2.0.CO;2

Wyrtki, K. (1986). Water displacements in the Pacific and the genesis of El Niño cycles. *Journal of Geophysical Research*, *91*, 7129–7132.

Yu, Y., Dommenget, D., Frauen, C., Wang, G., & Wales, S. (2016). ENSO dynamics and diversity resulting from the recharge oscillator interacting with the slab ocean. *Climate Dynamics*, *46*(5-6), 1665–1682. https://doi.org/10.1007/s00382-015-2667-1